NANO LETTERS

LETTER

pubs.acs.org/NanoLett

# Enhancing the Curie Temperature of Ferromagnetic Semiconductor (Ga,Mn)As to 200 K via Nanostructure Engineering

Lin Chen,[†] Xiang Yang,[†] Fuhua Yang,[†] Jianhua Zhao,[†,*] Jennifer Misuraca,[§] Peng Xiong,[§] and Stephan von Molnár[§]

[†]State Key Laboratory for Superlattices and Microstructures, Institute of Semiconductors, Chinese Academy of Sciences, P.O. Box 912, Beijing 100083, China

[§]Department of Physics, Florida State University, Tallahassee, Florida 32306, United States

Supporting Information

**ABSTRACT:** We demonstrate by magneto-transport measurements that a Curie temperature as high as 200 K can be obtained in nanostructures of (Ga,Mn)As. Heavily Mn-doped (Ga,Mn)As films were patterned into nanowires and then subject to low-temperature annealing. Resistance and Hall effect measurements demonstrated a consistent increase of $T_C$ with decreasing wire width down to about 300 nm. This observation is attributed primarily to the increase of the free surface in the narrower wires, which allows the Mn interstitials to diffuse out at the sidewalls, thus enhancing the efficiency of annealing. These results may provide useful information on optimal structures for (Ga,Mn)As-based nanospintronic devices operational at relatively high temperatures.

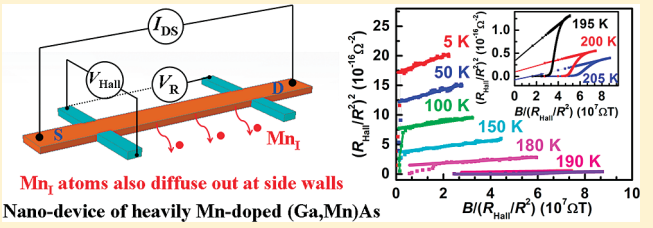


**KEYWORDS:** Magnetic semiconductors, magnetic properties of nanostructures, magnetotransport phenomena, molecular-beam epitaxy

In the past decade, (Ga,Mn)As[1,2] has served as a prototype diluted magnetic semiconductor in which to test concepts for spintronic applications and general methods for enhancing magnetic exchange in utilitarian semiconductors of the III−V group. Many important spintronic functionalities have been realized based on this material,[3] including electrical-field control of the Curie temperature $T_C$[4−6] and the magnetization,[7] spin injection into nonmagnetic semiconductors,[8] tunneling magneto-resistance[9] and electric current induced magnetization reversal.[10,11] However, all of the device operations were demonstrated at temperatures much below room temperature. For practical applications, increasing $T_C$ beyond room temperature is a necessity. The highest $T_C$ obtained on (Ga,Mn)As to date is 191 K;[12] thus exploring various routes of raising this value is of great fundamental and practical significance.

According to the p-d Zener model, $T_C$ of (Ga,Mn)As can be expressed as $T_C = [(N_{Mn}s(s + 1))/(3k_B)][(J_{pd}^2\chi_f)/((g\mu_B)^2)]$, where $N_{Mn}$ is the density of $Mn^{2+}$ ions which substitute into the Ga sites, $s$ is the $Mn^{2+}$ spin, $J_{pd}$ is the p-d exchange integral, $\chi_f$ is the free carrier susceptibility, $k_B$ is the Boltzmann constant, $g$ is the g-factor, and $\mu_B$ is the Bohr magneton.[13,14] The expression reveals two general approaches to increase $T_C$. One is increasing the effective Mn density, which provides both the localized magnetic moments and the holes mediating the ferromagnetic coupling. The other is decreasing self-compensating Mn interstitials, which act as double donors and compensate a significant fraction of the free holes. There are several proposals for enhancing $T_C$ to or above room temperature, such as using high-index substrates to increase the effective Mn concentration,[15,16] and codoping of donors to reduce the self-compensating Mn interstitials.[17−19] The present investigation is inspired by and effectively combines two proven approaches for increasing $T_C$ of (Ga,Mn)As: heavy Mn doping to increase the effective Mn concentration[12,20−22] and nanoscale patterning to increase the efficiency of postgrowth annealing.[23,24]

On one hand, by optimizing low-temperature growth conditions, Mn as high as 20% can be alloyed into GaAs without inducing phase separation.[12,20−22] The heavy Mn incorporation is an effective way of increasing the level of Mn substitution of Ga and has resulted in the improvement of $T_C$ from 165 to 191 K. However, heavy Mn incorporation inevitably leads to a large fraction of Mn interstitials which counteract the effects of the substitutional Mn atoms. On the other hand, it has been shown that $T_C$ of a GaAs-capped (Ga,Mn)As layer with moderate Mn-doping (∼6%) can be enhanced via a combination of nanopatterning and annealing.[23,24] It was postulated that nanostructures facilitate the diffusion of Mn interstitials toward sidewalls, thus enhances the effect of annealing. This scheme is expected to be even more effective in samples with heavy Mn doping because of the larger density of Mn interstitials. In this

**Received:** November 4, 2010
**Revised:** June 8, 2011
**Published:** June 22, 2011

work, we combined these two approaches to enhance $T_C$ of (Ga,Mn)As. $T_C$ as high as 200 K was obtained after low-temperature annealing of patterned nanowires of highly Mn-doped (Ga,Mn)As, which was evidenced through both temperature-dependent resistance data and Arrott plots derived from the anomalous Hall effect measurements. Our results reveal the potential for further increases of $T_C$ in this important material.

The heavily Mn-doped (Ga,Mn)As film with a thickness of 10 nm used for nanowire patterning in this study was grown on a rotating semi-insulating GaAs (001) substrate by low-temperature molecular-beam epitaxy (LT-MBE) at 200 °C. During growth, the V/III beam equivalent pressure ratio was set to 8. A clear streaky (1 × 2) surface reconstruction pattern was monitored by reflection high-energy electron diffraction (RHEED), showing two-dimensional growth mode. The details for reproducible growth of these kinds of high-quality (Ga,Mn)As films have been reported in ref 12.

The nominal Mn concentration, $x_{nomi}$, of the film was estimated by high-resolution X-ray diffraction (HRXRD).[25] According to Vegard's law, the lattice constant $a = 0.566(1 - x) + 0.598x$ nm. Here, $a = 0.566$ nm for $x = 0$ is the lattice constant of GaAs grown at low temperature, and $a = 0.598$ nm for $x = 1$ is the lattice constant of hypothetical zincblende MnAs. Because the (Ga,Mn)As layer is fully strained on GaAs, the free-standing lattice constant of (Ga,Mn)As can be calculated from the formula[26] $a = [(1 - \nu)/(1 + \nu)]a_{XRD} + [(2\nu)/(1 + \nu)]a_{GaAs}$, where $a_{XRD}$ is the measured lattice constant, $a_{GaAs}$ is the lattice constant of GaAs, and $\nu$ is the Poisson ratio. Figure 1a shows the $\omega$-$2\theta$ scan of the film used for patterning near the GaAs (004) peak of the substrate. The nominal Mn concentration $x_{nomi}$ is estimated to be 16.2% for the as-grown state and decreases to 13.0% after annealing in air at 160 °C for 13 h. In order to establish the evolution of the magnetic properties of the film with annealing, eight pieces were cut from the same wafer and annealed at 160 °C for various durations of time. Magnetic measurements were performed on each sample with a commercial superconducting quantum interference device (SQUID) magnetometer. Figure 1b shows a set of temperature dependent remnant magnetization curves for the film in the as-grown state and at various annealing times. Figure 1c summarizes the $T_C$ as a function of annealing time. We can see that $T_C$ reaches a maximum after annealing for 2 h and stays at this value even after annealing for 46 h, which shows the absence of any detrimental effect from over annealing in this sample at this annealing temperature. Magnetic hysteresis measurements show a hard magnetic axis perpendicular to the plane due to compressive strain; the in-plane magnetic easy axis is along the [−110] direction. The low-temperature annealing process reduces the Mn interstitial density and improves the quality of the (Ga,Mn)As, that is, increasing its hole density, magnetic moment, and $T_C$.[27,28] The effective Mn concentration, $x_{eff}$, of the annealed sample was 8.6% based on the saturation magnetization $M_s$ at 5 K and the assumption of $S = 5/2$ for each substitutional Mn ($Mn_{Ga}$) atom which participates in the hole-induced ferromagnetism. This is much smaller than $x_{nomi}$ = 13.0% determined by HRXRD and means the Mn interstitials have not been entirely removed.

The nanowire devices used for the magnetotransport measurements were fabricated in two steps. First, a standard Hall bar with width and length of 5 and 10 $\mu$m, respectively, was produced by optical lithography and wet etching by a solution of $H_3PO_4$/$H_2O_2$/$H_2O$ = 1:1:38. Then a nanowire structure with desired width was defined on top of the active channel of the large Hall

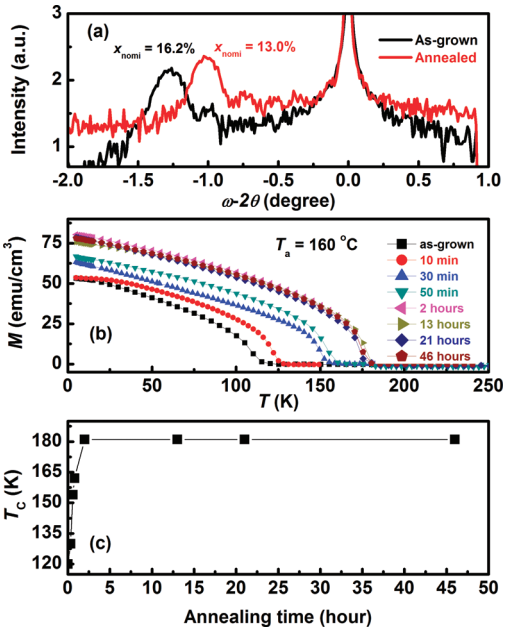


**Figure 1.** (a) $\omega$-$2\theta$ scan near the GaAs (004) substrate peak. (b) Temperature dependent remnant magnetization curves of 8 samples of unpatterned films from the same wafer which was used for patterning nanowires in the study. They have been subject to different annealing times as indicated at the same annealing temperature of 160 °C. (c) The Curie temperature as a function of the post annealing time.

bar by electron-beam lithography, using 200 nm thick polymethylmethacrylate (PMMA) resist and a MIBK/IPA = 3:1 developer. The pattern was transferred from PMMA to the (Ga,Mn)As layer by wet etching in the same etching solution. All the devices were patterned so that the lengths of the nanowires are oriented along the [110] direction. During the patterning process, all samples were subject to the same thermal treatments, and the highest baking temperature was 110 °C. Figure 2a−d shows several typical scanning electron microscopy (SEM) images of the nanodevices with channel widths from 156 to 686 nm.

Because the magnetic moment of each nanowire is minute compared to that of the larger connecting structures and too small to be detected by the SQUID magnetometer, we determined $T_C$ by using transport measurements carried out in a physical property measurement system (PPMS). The magnetotransport measurements were performed with the magnetic field $B$ perpendicular to the sample plane. The Hall resistance $R_{Hall}$ and longitudinal resistance $R$ were measured by standard four-probe method. To avoid any Joule heating, a bias current $I$ = 50 nA was used in all the measurements.

Since the temperature dependence of the resistance, especially the well-defined peak near the ferromagnetic transition, has been widely used to determine $T_C$ in (Ga,Mn)As,[23,28,29] we first probed $T_C$ by measuring the resistance as a function of temperature. The positions of the resistance peaks were determined from the derivatives of $R(T)$ by calculating the temperature at which $dR/dT = 0$. On the basis of the theory of Fisher and Langer,[30] the position of $T_C$ on the $R(T)$ curve is dependent on the magnitude of the wave vector of the carriers (carrier density). In the case of (Ga,Mn)As, whose carrier density lies in between the extremes for insulating concentrated magnetic semiconductors and ferromagnetic metals, the location of $T_C$ on the $R(T)$ curve has been found to be sample dependent: in some samples $T_C$ is located at


dx.doi.org/10.1021/nl201187m |Nano Lett. 2011, 11, 2584–2589

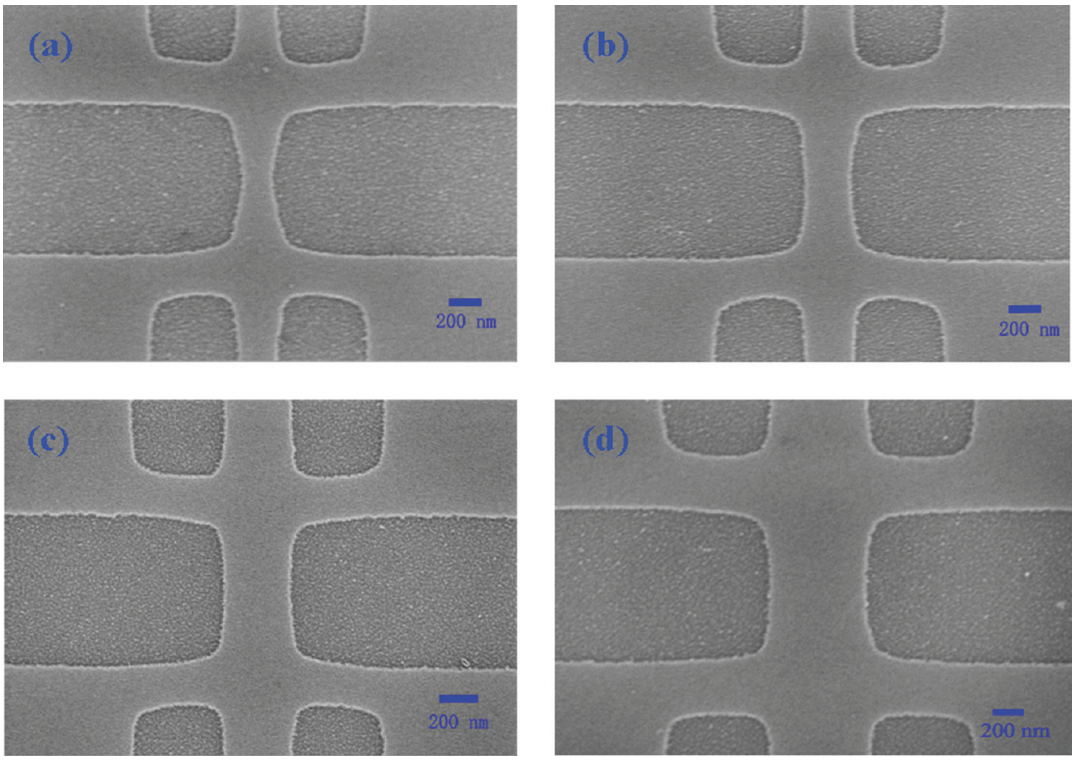


**Figure 2.** Scanning electron microscopy images of the nanowire devices with widths of 156 nm (a), 255 nm (b), 310 nm (c), and 686 nm (d). All the Hall bars were patterned such that the lengths are oriented along the [110] direction.

the resistance peak ($dR/dT = 0$)[23,28,29] while in others at the maximum for $dR/dT$.[29] Therefore, for a particular set of samples, it is crucial to establish experimentally the proper criterion for $T_C$ determination from $R(T)$. We have done so for our heavily Mn-doped continuous film, via direct comparison of the temperature dependent magnetization and resistance measurements on the same sample. The results are shown in Figure S1 (Supporting Information). It is clear that the $T_C$ determined from $M(T)$ coincides with the peak in $R(T)$ ($dR/dT = 0$), which provided the basis for using $dR/dT = 0$ as the criterion for determining $T_C$ in our samples. For the nanowires, we further provided a rigorous and independent confirmation of the value of $T_C$ by Arrott plots[25] derived from the anomalous Hall effect. Finally, we demonstrate in Figure S2 (Supporting Information) that the temperature dependencies of the resistivity are identical when measured along different crystalline orientations despite the strong in-plane magnetic anisotropy in the heavily Mn-doped (Ga,Mn)As film.

Figure 3 shows the temperature dependence of the resistance of a nanowire device with 310 nm width. It shows metallic behavior which is similar to a conventional metallic (Ga,Mn)As film. Below about 35 K, the resistance shows an upturn, probably due to electron−electron interactions.[31] $T_C$ of the as-made device, as determined by the resistance peak of the $R-T$ curve,[23,28] increases to 167 ± 5 K, up from 125 K for the as-grown film (shown in Figure 1b). This is most likely due to unintentional annealing during the sample processing.

Figure 4a shows the temperature dependent resistance curves of a number of as-made devices with different widths, and $T_C$ for each device is summarized in Figure 4c. We can see that the resistance increases monotonically as the width decreases, and $T_C$ is nearly the same for different widths (from 156 nm to 5 $\mu$m); no obvious quantum confinement effect was observed in this size

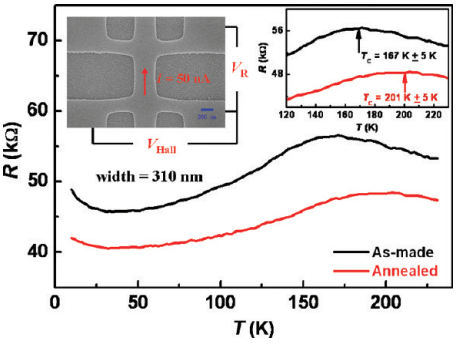


**Figure 3.** Temperature dependence of the resistance of a device with $w$ = 310 nm in the as-made (black) state and after annealing (red). Left inset shows the experimental geometry. Right inset shows the close-up view around $T_C$. All the measurements were done with a current $I$ = 50 nA.

regime. Figure 4b shows the temperature dependence of the resistance of the same devices after annealing in air at 160 °C for 13 h. $T_C$ values for the annealed samples, as determined from the resistance maximum of the $R-T$ curves, are summarized in Figure 4c. $T_C$ is increased to more than 190 K for the devices from 255 to 686 nm. This is in comparison to the device with 5 $\mu$m width, which has a $T_C$ of ∼180 K, similar to the $T_C$ determined from the SQUID magnetization measurement for the unpatterned film (Figure 1b). The $T_C$ enhancement reaches a maximum at wire width of about 310 nm, where $T_C$ is increased to as high as 201 ± 5 K as evidenced by $R-T$ measurements (also shown in Figure 3). At even smaller wire widths, $T_C$ decreases from this highest value.

To eliminate the possibility that the variation of $T_C$ with wire width is an artifact caused by under or over annealing of the wires,


dx.doi.org/10.1021/nl201187m |Nano Lett. 2011, 11, 2584–2589

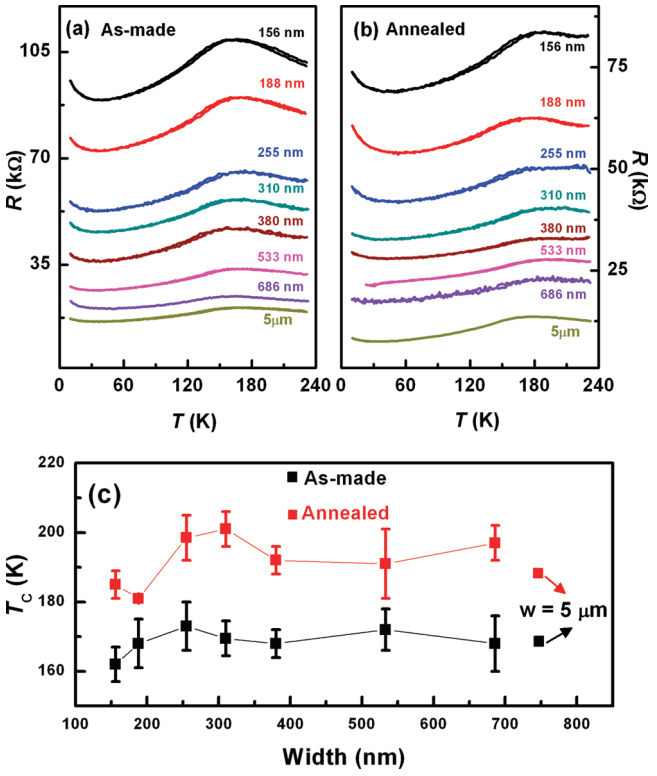


**Figure 4.** Temperature dependence of the resistance of several devices with different widths in the as-made (a) and annealed (b) states. $T_C$ values determined from the resistance maximum of $R-T$ curves are summarized in (c).

two series of nanowire devices with widths of 233 and 310 nm were fabricated and each device annealed at 160 °C for various durations. As shown in Figure 5a,b, for both groups of devices 13 h of annealing was sufficient to reach saturation and additional annealing did not cause any $T_C$ degradation. This is qualitatively consistent with the trend shown in Figure 1c for the unpatterned films and demonstrates that all the devices were optimally annealed.

We attribute the observed $T_C$ enhancement in the nanowires to the increase of the free surface, which allows the Mn interstitials to diffuse out at the sidewalls, thus enhancing the efficiency of annealing. Considering the geometry of the devices, length $l$, width $w$, and height $h$, the increased free surface at sidewalls is $2lh$. The percentage increase in the free surface is $2lh/lw = 6\%$ for $h = 10$ nm and $w = 310$ nm, while for the device with 5 $\mu$m width the free surface only increases by 0.4%. We show here that the free surface increase of 6% at sidewalls is important for the annealing of (Ga,Mn)As, which results in a 11% $T_C$ increase (from 180 to 200 K). We conclude that the nanostructure patterning greatly enhances the effect of thermal annealing. For the narrowest devices with widths of 156 and 188 nm, which have even larger free surface increases, the increase of $T_C$ after annealing is less than those of the devices with more moderate widths (255 and 310 nm). We surmise that this is due to strain relaxation induced by the lithographic patterning and annealing when the width becomes less than 200 nm,[32] which could degrade the crystalline quality of (Ga,Mn)As. To confirm that strain relaxation was indeed responsible for the $T_C$ reduction in the narrowest wires, we fabricated and measured a series of nanowires patterned from another piece of film that had been optimally annealed at 160 °C for 13 h. The nanowires underwent no additional annealing

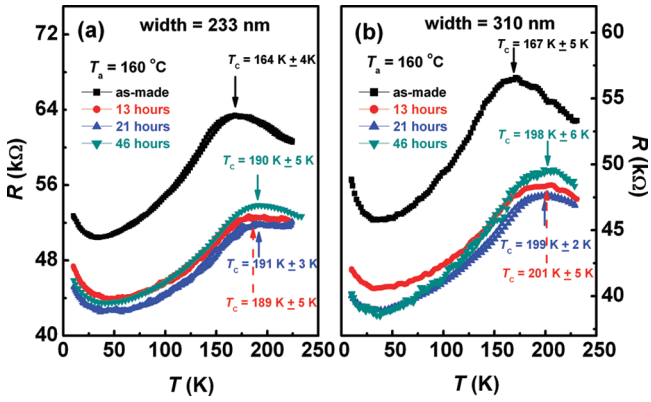


**Figure 5.** Temperature dependent resistance curves of two series of nanowires with widths of 233 nm (a) and 310 nm (b) in the as-made state and after different annealing times as indicated.

after patterning and care was taken to avoid any unintentional annealing during the patterning process (the baking temperature never exceeded 110 °C). The results are shown in Figure S3 (Supporting Information). No $T_C$ enhancement is seen with decreasing wire width, and a small reduction of $T_C$ (about 5–7 K) is observed when the width becomes smaller than 500 nm. These results convincingly demonstrate that strain relaxation induced by the lithographic patterning would decrease $T_C$. Furthermore, several other nanowire devices based on (Ga,Mn)As films of different thicknesses and Mn concentrations have been fabricated. The nanowires from a thicker (18 nm) (Ga,Mn)As film with similar heavy Mn-doping ($x_{nomi} = 14.3\%$) exhibit maximum $T_C$ enhancement quantitatively consistent with the results presented above; in contrast, for the moderately Mn-doped (Ga,Mn)As film ($x_{nomi} = 7.5\%$), the magnitude of $T_C$ enhancement is significantly smaller than that in either of the heavily Mn-doped (Ga,Mn)As samples. Detailed information on the effects of thickness and Mn concentration will be reported elsewhere.

In discussing Figure 3, we alluded to the fact that determining $T_C$ from the $R-T$ curve is not ideal with an error bar of several K. Here, we used Arrott plots to accurately determine $T_C$ beyond any ambiguity. The magnetic field dependence of the Hall resistance $R_{Hall}$ and resistance $R$ measured at different temperatures is shown in Figure 6a,b. The Hall resistance of (Ga,Mn)As can be written as $R_{Hall} = R_oB/d + R_sM/d$, where $R_o$ is the ordinary Hall coefficient, $R_s$ is the anomalous Hall coefficient, $d$ is the sample thickness, and $B$ and $M$ are the magnetic induction and magnetization perpendicular to the sample surface, respectively.[3] The anomalous Hall component is the dominant one at low field, and a scaling relation $R_S/d = cR^2$ ($c$ is a constant) is expected due to the dominance of the Berry-phase mechanism in the metallic regime.[33−35] Thus, the ratio of $R_{Hall}/R^2$ can be used to track the magnetization. In the Arrott plots, $(R_{Hall}/R^2)^2$ versus $B/(R_{Hall}/R^2)$, a ferromagnetic state corresponds to a positive extrapolated ordinate intercept, while paramagnetic state corresponds to a negative extrapolated intercept.[25,36] In Figure 6c, the extrapolated intercept remains positive at 200 K and turns negative at 205 K, indicating that $T_C$ is between those extrema and somewhat higher than 200 K. We point out that due to the very small magnetoresistance in the relevant temperature range (Figure 6b), the use of a different


dx.doi.org/10.1021/nl201187m |Nano Lett. 2011, 11, 2584–2589

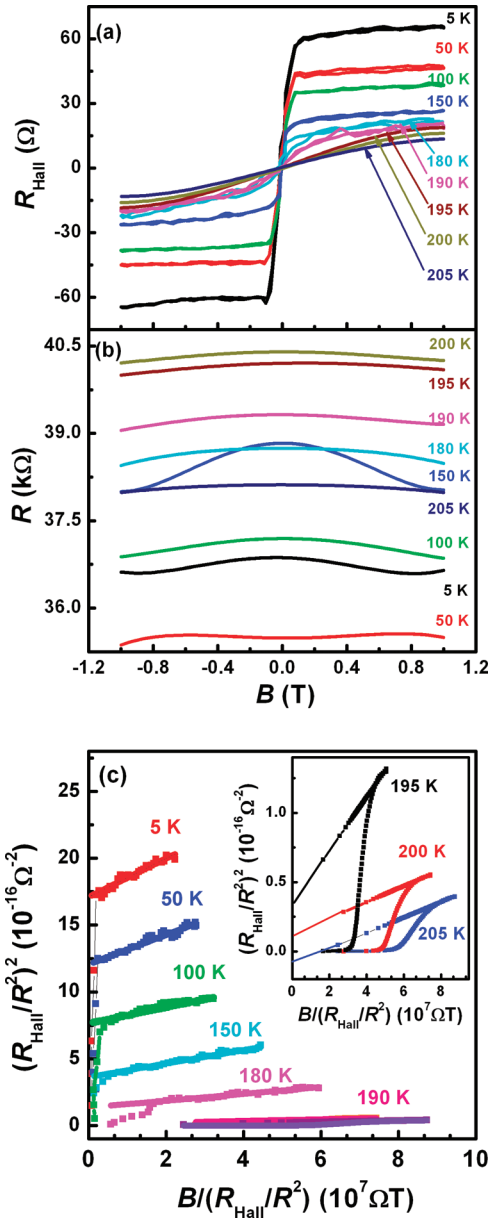


**Figure 6.** Magnetic field dependence of the Hall resistance (a) and resistance (b) of the annealed device with $w$ = 310 nm measured at different temperatures. (c) Arrott plots at different temperatures. The inset in (c) shows a close-up view of the Arrott plots near the ferromagnetic transition, which confirms $T_C$ is slightly above 200 K.

scaling relation has negligible effect on the outcome of the Arrott analysis.

In summary, $T_C$ up to 200 K was achieved by patterning a heavily Mn-doped (Ga,Mn)As thin film into nanostructures. Patterning the (Ga,Mn)As film into nanowires increases the free surface and allows the Mn interstitials to diffuse out at the sidewalls, thus enhancing the efficiency of annealing. Much higher $T_C$ could be expected by optimizing the annealing condition of the nanodevices and by using a film with higher preannealed $T_C$. These results may provide a useful design guideline for optimal dimensions for (Ga,Mn)As-based nanospintronic devices operating at higher temperatures.

## ■ ASSOCIATED CONTENT

**Ⓢ Supporting Information.** Additional information and figures. This material is available free of charge via the Internet at http://pubs.acs.org.

## ■ AUTHOR INFORMATION

**Corresponding Author**
*E-mail: jhzhao@red.semi.ac.cn.

## ■ ACKNOWLEDGMENT

The authors acknowledge H. Z. Zheng and J. J. Deng for useful discussions, X. Z. Yu, H. L. Wang, S. H. Nie, P. F. Xu, S. L. Wang, K. K. Meng, and L. J. Zhu for their help on sample preparation, and H. Y. Yu and J. Yan for magneto-transport measurements. This work is supported in part by the National Natural Science Foundation of China under Grants 60836002 and 10920101071 and the special funds for the Major State Basic Research Contract No. 2007CB924903 of China, and the Knowledge Innovation Program Project of Chinese Academy of Sciences Grant No. KJCX2.YW.W09-1. S.v.M. and P.X. acknowledge NSF Materials World Network Grant DMR-0908625.

## ■ REFERENCES

(1) Ohno, H.; Shen, A.; Matsukura, F; Oiwa, A; Endo, A; Katsumoto, S; Iye, Y. *Appl. Phys. Lett.* **1996**, *69*, 363.
(2) *Semiconductors and semimetals: Spintronics*; Dietl, T., Awschalom, D. D., Kaminska, M., Ohno, H., Eds.; Elsevier: Oxford, 2008.
(3) Dietl, T; Ohno, H; Matsukura, F. *IEEE Trans. Electron Devices* **2007**, *54*, 945.
(4) Chiba, D; Yamanouchi, M; Matsukura, F; Ohno, H. *Science* **2003**, *301*, 943.
(5) Chiba, D; Matsukura, F; Ohno, H. *Appl. Phys. Lett.* **2006**, *89*, 162505.
(6) Sawicki, M; Chiba, D; Korbecka, A; Nishitani, Y; Majewski, J. A; Matsukura, F; Dietl, T; Ohno, H. *Nat. Phys.* **2009**, *6*, 22.
(7) Chiba, D; Sawicki, M; Nishitani, Y; Nakatani, Y; Matsukura, F; Ohno, H. *Nature (London)* **2008**, *455*, 515.
(8) Ohno, Y; Young, D. K; Beschoten, B; Matsukura, F; Ohno, H; Awschalom, D. D. *Nature (London)* **1999**, *402*, 790.
(9) Tanaka, M; Higo, Y. *Phys. Rev. Lett.* **2001**, *87*, 026602.
(10) Chiba, D; Sato, Y; Kita, T; Matsukura, F; Ohno, H. *Phys. Rev. Lett.* **2004**, *93*, 216602.
(11) Yamanouchi, M; Chiba, D; Matsukura, F; Ohno, H. *Nature (London)* **2004**, *428*, 539.
(12) Chen, L; Yan, S; Xu, P. F; Lu, L; Wang, W. Z; Deng, J. J; Qian, X; Ji, Y; Zhao, J. H. *Appl. Phys. Lett.* **2009**, *95*, 182505.
(13) Dietl, T; Ohno, H; Matsukura, F; Cibert, J; Ferrand, D. *Science* **2000**, *287*, 1019.
(14) Dietl, T; Ohno, H; Matsukura, F. *Phys. Rev. B* **2001**, *63*, 195205.
(15) Wang, K. Y; Edmonds, K. W; Zhao, L. X; Sawicki, M; Campion, R. P; Gallagher, B. L; Foxon, C. T. *Phys. Rev. B* **2005**, *72*, 115207.
(16) Wurstbauer, U; Sperl, M; Soda, M; Neumaier, D; Schuh, D; Bayreuther, G; Zweck, J; Wegscheider, W. *Appl. Phys. Lett.* **2008**, *92*, 102506.
(17) Wang, W. Z; Deng, J. J; Lu, J; Chen, L; Ji, Y; Zhao, J. H. *Physica E* **2008**, *41*, 84–87.
(18) Cho, Y. J; Yu, K. M; Liu, X; Walukiewicz, W; Furdyna, J. K. *Appl. Phys. Lett.* **2008**, *93*, 262505.
(19) Schott, G. M; Rüster, C; Brunner, K; Gould, C; Schmidt, G; Molenkamp, L. W; Sawicki, M; Jakiela, R; Barcz, A; Karczewski, G. *Appl. Phys. Lett.* **2004**, *85*, 4678.

(20) Chiba, D; Nishitani, Y; Matsukura, F; Ohno, H. *Appl. Phys. Lett.* **2007**, *90*, 122503.
(21) Ohya, S; Ohno, K; Tanaka, M. *Appl. Phys. Lett.* **2007**, *90*, 112503.
(22) Mack, S; Myers, R. C; Heron, J. T; Gossard, A. C; Awschalom, D. D *Appl. Phys. Lett.* **2008**, *92*, 192502.
(23) Eid, K. F; Sheu, B. L; Maksimov, O; Stone, M. B; Schiffer, P; Samarth, N. *Appl. Phys. Lett.* **2005**, *86*, 152505.
(24) Sheu, B. L; Eid, K. F; Maksimov, O; Samarth, N; Schiffer, P. *J. Appl. Phys.* **2006**, *99*, 08D501.
(25) Ohno, H. *Science* **1998**, *281*, 951.
(26) *Semiconductor Spintronics and Quantum Computation*; Awschalom, D. D., Loss, D., Sarmarth, N., Eds.; Springer: Berlin, 2002.
(27) Yu, K. M; Walukiewicz, W; Wojtowicz, T; Kuryliszyn, I; Liu, X; Sasaki, Y; Furdyna, J. K. *Phys. Rev. B* **2002**, *65*, 201303(R).
(28) MacDonald, A. H; Schiffer, P; Samarth, N. *Nat. Mater.* **2005**, *4*, 195.
(29) Novák, V; Olejník, K; Wunderlich, J; Cukr, M; Výborný, K; Rushforth, A. W.; Edmonds, K. W.; Campion, R. P; Gallagher, B. L; Sinova, J; Jungwirth, T. *Phys. Rev. Lett.* **2008**, *101*, 077201.
(30) Fisher, M. E; Langer, J. S. *Phys. Rev. Lett.* **1968**, *20*, 665.
(31) Neumaier, D; Schlapps, M; Wurstbauer, U; Sadowski, J; Reinwald, M; Wegscheider, W; Weiss, D. *Phys. Rev. B* **2008**, *77*, 041306(R).
(32) Wenisch, J; Gould, C; Ebel, L; Storz, J; Pappert, K; Schmidt, M. J; Kumpf, C; Schmidt, G; Brunner, K; Molenkamp., L. W *Phys. Rev. Lett.* **2007**, *99*, 077201.
(33) Jungwirth, T; Niu, Q; MacDonald, A. H. *Phys. Rev. Lett.* **2002**, *88*, 207208.
(34) Chun, S. H; Kim, Y. S; Choi, H. K; Jeong, I. T; Lee, W. O; Suh, K. S; Oh, Y. S; Kim, K. H; Khim, Z. G; Woo, J. C; Park, Y. D. *Phys. Rev. Lett.* **2007**, *98*, 026601.
(35) Pu, Y; Chiba, D; Matsukura, F; Ohno, H; Shi, J. *Phys. Rev. Lett.* **2008**, *101*, 117208.
(36) Arrott, A *Phys. Rev.* **1957**, *108*, 1394.